Endotoxin Removal from Biopharmaceuticals and Vaccines by an Antimicrobial Peptide-Based Affinity Matrix: a Kinetics Study

Mina Sepahi, Shahin Hadadian*, Reza Ahangari Cohan, Dariush Norouzian

Nano-Biotechnology Department, New Technologies Research Group, Pasteur Institute of Iran, Tehran, 1316943551, Iran.

ARTICLE INFO

*Corresponding Authors:
Shahin Hadadian;
Nanobiotechnology Department, New Technologies Research Group, Pasteur Institute of Iran, Tehran, 1316943551, Iran.
Email: hadadian@pasteur.ac.ir
Tel/Fax: +98-21-64112216

ABSTRACT

Introduction: Endotoxin removal is a crucial stage in ensuring the safety of parenteral products. S3E3-S-Sepharose, which has been generated via site-specific immobilization of the S3E3 cationic amphiphilic peptide (CAP) on Sepharose, is a newly designed affinity matrix proposed for lipopolysaccharide (LPS) removal from biopharmaceuticals and vaccines. **Methods:** In the current study, the kinetic behavior of LPS adsorption on the matrix was investigated at pHs 4.5 and 8.5 by incubation of LPS-contaminated bovine serum albumin (BSA) solutions, as a model, with the S3E3-Sepharose matrix at different incubation times in a batch-wise mode. Various mathematic models were employed to explain the amount of adsorbed LPS, and the normalized root mean square error (NRMSE), relative prediction error (RE), and relative percentage error (RPE) were utilized to identify the best-fitting model. **Results:** The kinetics study revealed that the pseudo-second-order (PSO) reaction, and pore diffusion mass transfer were the rate-controlling steps of LPS adsorption on the S3E3-S-Sepharose and pH of samples did not affect the LPS adsorption kinetics. **Conclusion:** These findings provide valuable insights for scaling up the LPS removal process through affinity chromatography, contributing to advances in biopharmaceutical and vaccine production research.

INTRODUCTION

Safety is the most critical attribute of quality for any injectable drug or vaccine. One key aspect of safety is ensuring that the injectable product is free from pyrogenic agents [1]. Although the lipopolysaccharide of Gram-negative bacteria is not the only pyrogenic agent in parenteral products, it is often considered the main source of pyrogenic contamination due to high pyrogenic activity, the ubiquity presence in nature, resistance to sterilization, and remaining in solutions even after filtration [2, 3]. Endotoxin can be removed from biopharmaceuticals by chromatographic methods, especially by ion exchange and affinity chromatography, if the limitations related to the pH, conductivity, and the difference between isoelectric point of target biomolecule and endotoxin are taken into account [4, 5]. Affinity chromatography matrices conjugated with certain amphiphilic cationic antimicrobial peptides (AMPs) can effectively remove LPS from protein solutions at different conditions [6, 5, 7]. The S3E3-S-Sepharose affinity matrix is a good example of AMP-based LPS removal affinity matrices. S3E3 is a modified analog of linear S3 antimicrobial peptide derived from the LPS binding site of factor C of horseshoe crab hemolymph. The net positive charge of S3E3 CAP was increased by removing 3 negatively charged glutamic acid residues of S3 peptide [8]. In our previous study, S3E3-S-Sepharose affinity matrix was generated by chemo-selective immobilization of S3E3 cationic antimicrobial peptide on activated Sepharose 6%

containing iodoacetyl linkers via a thioether bond [5]. S3E3-S-Sepharose was applied for effective LPS-removal from bovine surum albomin [9].

However, due to the difference in physicochemical properties of proteins, it is necessary to optimize the operating conditions for each target to obtain maximum performance. Static adsorption capacity is one of the most useful preliminary measures for evaluating the efficiency of chromatography matrices. The static binding capacity of an adsorbent is obtainable at a batch equilibrium state. The time needed for reaching the adsorption equilibrium state and the adsorption behavior of adsorbents can be determined by performing the adsorption study at different time intervals. Adsorption kinetics provide crucial information about the mechanism of adsorption and rate-controlling steps. Adsorption of any adsorbate to adsorbents may occur through a physisorption or chemisorption mechanism and the rate of adsorption may be limited by reaction kinetics and/or mass transport phenomena.

Mass transport of an adsorbate toward the porous adsorbents consists of different steps including, adsorbate moving from the bulk of solution toward the external surface of adsorbent particles (external diffusion), diffusion through the thin liquid film layer surrounding the surface of the adsorbent particles (film diffusion), and diffusion inside the intraparticle spaces and pores of the adsorbent (pore diffusion) to find vacant reaction sites [10,

11]. One or some of these steps usually control the rate of adsorption. Although the equilibrium states of LPS adsorption in some affinity matrices have been studied [12-16], an overview of adsorption rate-controlling steps of LPS adsorption on affinity matrices is not available. In the current study, we investigate the kinetics behaviour of LPS adsorption on S3E3-S-Sepharose at two different pHs of 4.5 and 8.5. Finally, the rate-controlling mechanism of LPS adsorption on the S3E3-Sepharose matrix was investigated by different statistical modelling.

MATERIALS AND METHODS

Affinity Matrix Preparation

S3E3-S-Seph arose affinity matrix was prepared by immobilizing S3E3 peptide (H A H K V K I G V Q K Y G Q F P Q G T V T Y T C S G N Y F L) on 6% cross-linked Sepharose containing iodoacetyl linkers (Cat. 786-805, G- Biosciences, USA) according to our previous work [5]. Then, two affinity columns were prepared by pouring 1 ml of gel into each column. To study the kinetics of LPS adsorption at different pHs, one column was equilibrated with 10 ml of 10 mM Tris-HCl buffer (pH 8.5) and the other was equilibrated with 10 ml of 50 mM sodium acetate buffer (pH 4.5).

Kinetics Models for LPS Adsorption in the Batch Mode

To estimate the incubation time needed for batch-wise LPS removal and adsorption kinetics study, two different BSA samples (10 mg/mL) were prepared in 50 mM sodium acetate buffer (pH 4.5, Sample S1) and 10 mM Tris- HCl buffer (pH 8.5, Sample S2). Then, both samples were contaminated with $1.5 \times 10^{+5}$ EU LPS of *E. coli* 055: B5 (Cat. 2880, Sigma Aldrich, USA). Eighteen aliquots (1 mL) for each S1 and S2 sample were dispensed in 2.5 mL microtubes. Then, 50 µL equilibrated affinity gel was added to each microtube and incubated with mild shaking at room temperature at different time intervals (5-30 minutes). After centrifugation at 1000 g for 2 minutes, the LPS concentration in the supernatants was measured by Limulus amebocyte lysate (LAL) chromogenic kit (QCL-1000, Lonza, USA) to calculate the remaining LPS [17]. The amount of adsorbed LPS after a certain incubation time (t, minutes) was calculated according to the following equation [18]:

$$q_t \text{ (EU/mL of matrix)} = (C_0 - C_t) \times V / V_m \qquad (1)$$

Where q is the amount of adsorbed LPS per one milliliter of the matrix, C_0 and C are the initial LPS concentrations (EU/mL) of each sample and the LPS concentration of the supernatant of samples after t-minute incubation with affinity matrix. V and V_m (mL) represent the volume of the sample and the wet affinity matrix.

Elovich, pseudo-first-order (PFO), pseudo-second-order (PSO), intraparticle diffusion, and pore diffusion models were investigated to recognize the rate-controlling mechanism of LPS adsorption on the S3E3-Sepharose matrix. Elovich equation is given by [19, 10, 20-22]:

$$\frac{dq}{dt} = \delta e^{-\gamma q} \qquad (2)$$

Where δ is the initial adsorption rate [EU/ (mL matrix. min)] and γ is the desorption constant related to the activation energy for chemisorption and extent of surface coverage (mL matrix/EU). The linearized integrated form of the Elovich equation can be written as:

$$q_t = \frac{1}{\gamma} ln (t) + \frac{1}{\gamma} ln (\gamma\delta) \qquad (3)$$

PFO reaction rate model is expressed as [19, 10, 20-22]:

$$\frac{dq}{dt} = k_1(q_e - q_t) \qquad (4)$$

Where qe and q_t (absorbed EU/ ml resin) are the amount of adsorbed LPS to 1 mL of the matrix at equilibrium and time t. The term k_1 (min $^{-1}$) is the first-order apparent sorption rate constant. The linear form of integration of the pseudo-first-order equation is [19, 10, 20-22]:

$$\log (q_e - q_t) = - \frac{k_1}{2.303} t + \log(q_e) \qquad (5)$$

PSO model and its linearized integration can be expressed [10, 21, 18, 23, 24]:

$$\frac{dq}{dt} = k_2(q_e - q_t)^2 \qquad (6)$$

$$\frac{t}{q} = \frac{1}{k_2 q_e^2} + \frac{1}{q_e} t \qquad (7)$$

Where k_2 (ml EU^{-1} min $^{-1}$) is the rate constant of the PSO model.

In the kinetics study, mass transfer models including intraparticle diffusion (Weber and Morris' equation) and pore diffusion (Bangham's equation) were evaluated [10, 21, 25, 18, 24]. **Equation 8** represents the intraparticle diffusion model:

$$q = k_{id} t^{0.5} + C \qquad (8)$$

Where k_{id} and C are the rate constant and thickness boundary layer constant of the intraparticle diffusion model, respectively.

The linear form of the pore diffusion (Bangham) model can be written as:

$$\log \left(\log \left(\frac{C_0}{C_t} \right) \right) = \log \left(\frac{k_b \times Vm}{2.303 \times V} \right) + a \log(t) \qquad (9)$$

Where C_0 and C are the initial LPS concentrations (EU/ml) of each sample and the LPS concentration of the supernatant of samples after t-minute incubation with affinity matrix. V and V_m (ml) represent the volume of the sample and the wet affinity matrix. The term k_b is the Bangham constant, and "a" is the slope of the line.

The theoretical models were evaluated empirically and their goodness of fitting was determined by the coefficient of determination (R^2) obtained from fitting curves, and normalized root mean square error (NRMSE) according to the following equations [10, 25, 18, 26, 24]:

$$NRMSE = \frac{Root\ Mean\ Square\ Error\ (RMSE)}{average} = \frac{\sqrt{\frac{\Sigma_{i=1}^{n}\left(q_{i,emp} - q_{i,est}\right)^2}{n-2}}}{\frac{\Sigma_{i=1}^{n}(q_{i,emp})}{n}}$$

$$(10)$$

Where $q_{i,emp}$ and $q_{i, est}$ are the empirical and estimated values of the adsorbed LPS to 1 ml of the matrix at ith observation, n is the number of observations.

The relative percentage error (RPE) between experimental $q_{t30,emp}$ which was considered as q at the equilibrium state ($q_{e, emp}$) and estimated qe ($q_{e, est}$) obtained by model equation was calculated according to the following equation and was applied as an additional error function for selecting models [26].

$$RPE = \frac{(q_{e,emp} - q_{e,est})}{q_{e,emp}} \times 100 \qquad (11)$$

RESULTS

Empiric Model of LPS Adsorption

The equilibrium state of LPS adsorption on the S3E3-S-Sepharose affinity matrix was studied at two combinations of sample criteria including pH and LPS concentrations. The static binding capacity of the matrix (q) for removing LPS from the BSA solution after different contact times was determined. The values of q were plotted versus contact time (Fig. 1). The minimum time required for starting the plateau phase was considered batch mode incubation time [25]. For both S1 and S2 samples, the values of q increased sharply during the first 10 minutes indicating that the rate of the adsorption process was high at the early 10 minutes of the process, then slowed down between 10 to 15 minutes and were approximately constant from 15 up to 30 minutes. Thus, the amount of adsorbed LPS after 30 minutes of incubation ($q_{t30, emp}$) was considered empirical static binding capacities of the equilibrium state ($q_{e, emp}$). At pH 4.5, the value of $q_{e, emp}$ (2903475.2 EU/ml) was higher than $q_{e, emp}$ of pH 8.5 (2702439 EU/ml).
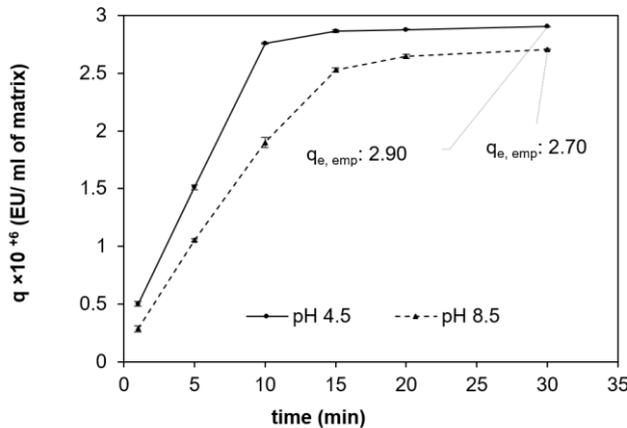

Fig. 1. Kinetics study for the static binding capacity of the S3E3-Sepharose matrix: Amount of adsorbed LPS per 1 milliliter of the matrix after different incubation times. For both pH 4.5 and pH 8.5 samples, the curves of empirical q (q_{emp}) showed a rapid increase before levelling off, which aligns with the typical behavior of exponential curves.

Chemisorption Model of LPS Adsorption

The Elovich model can explain the exponential behavior of LPS adsorption. According to Equation 3, the linearized equation of the Elovich model provided information about the initial rate of LPS adsorption to the matrix and desorption constant (Fig. 2a). By plotting the q versus ln t, the slope and intercept of the linear trend line crossing the data, were used to calculate the LPS adsorption initial rate (γ, EUml-1min) and LPS desorption constant (δ). Then the resulting Elovich model was applied to

estimate the q and to compare with correspondent empirical values of q (Fig. 2b).
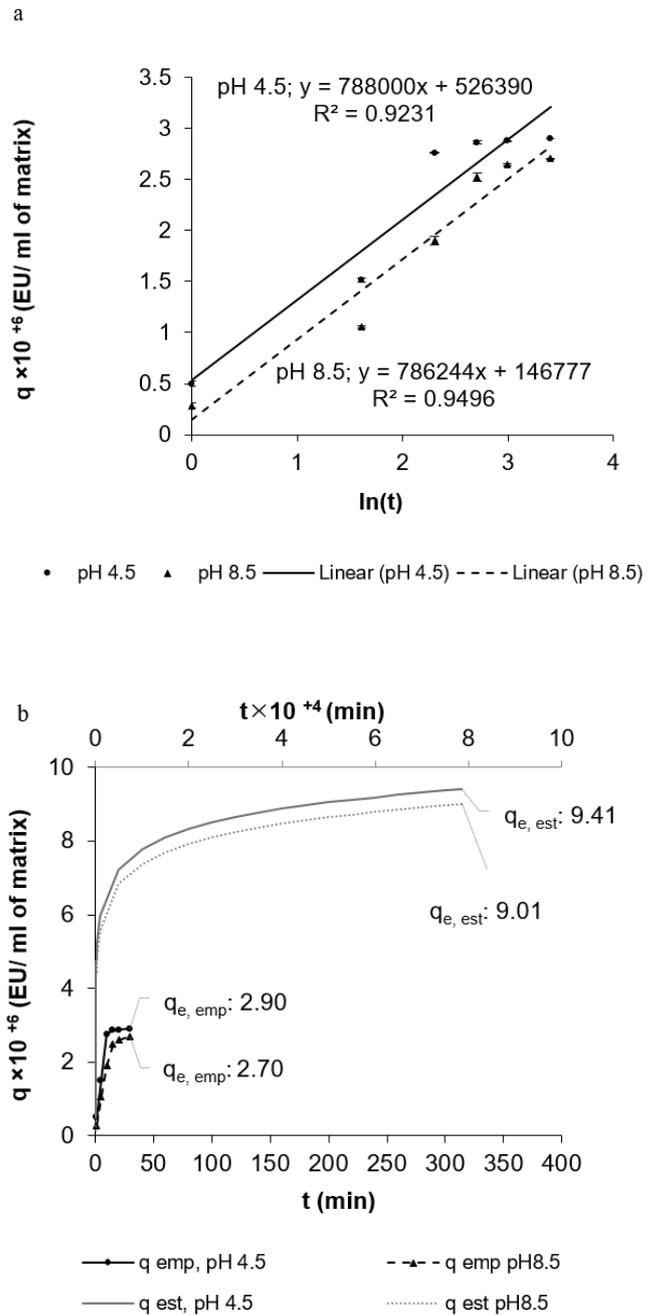
Fig. 2. Elovich model for kinetics study of LPS adsorption to S3E3-Sepharose matrix. a) Linearized Elovich model for LPS adsorption at pH 4.5 and 8.5: The trend lines passing data points had coefficients of determination (R^2) of more than 0.9 demonstrating appropriate fitting of the Elovich model and consequently, indicating the chemisorption mechanism of LPS adsorption. b) Comparison of Elovich model-estimated values with empirical data: By extrapolating the resulting Elovich models, the equilibrium state for pH 4.5 and 8.5 was estimated 9.41 $\times 10^{+6}$ and 9.01 $\times 10^{+6}$ EU/ml, respectively.

For both pH 4.5 and pH 8.5 samples, the linearized Elovich model demonstrated appropriate fitting to the empirical data with 0.92 and 0.95 of R^2, respectively. However, the estimated qe

determined by extrapolation of the Elovich model was higher than empirical values.

Models Based on Order of Adsorption Reaction

The fitness of the PFO and PSO reaction kinetic models was investigated to determine the order of chemical reactions involved in LPS adsorption to the matrix. According to Equation 5, the values of k_1 and q_e, est were determined by the slope and intercept of the equation of linear trend line obtained from plotting log (q_e, emp - q_t,emp) versus incubation time (Fig. 3a). After determining the terms of pseudo-first order reaction kinetics models for pH 4.5 and pH 8.5 samples, these models were applied for estimation of the values of q_t, est and the conformities of q_t, est of with corresponding empirical values (q_t,emp) were shown at Fig. 3b.
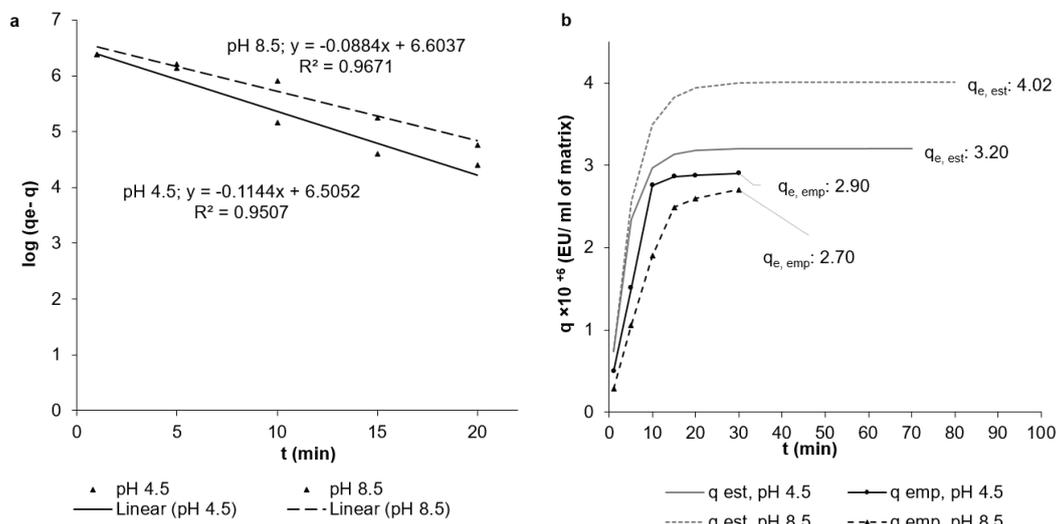
Fig. 3. Kinetic models for studying the reaction order of LPS adsorption. a) Linearized PFO reaction kinetics model. The intercept of the trend line was equal to log q_e, est. Thus, the values of q_e, est were calculated 10 6.6037 (4015133.6 EU/ml of the matrix) and 10 6.5052 (3200368.6 EU/ml of the matrix) for pH 8.5 and pH 4.5, respectively. b) Comparison of LPS adsorption PFO reaction kinetics model with empirical data. At both pHs, the q_e, est values were overestimated.

For the PSO model, the values of t/q were plotted versus t (Fig. 4a) and the slope (1/ $q_{e, est}$) and the intercept (1/ $k_2 q_{e, est}^2$) of the linear trend lines were used for calculating $q_{e, est}$ and k_2. The comparison of q_{est} values with the empirical data is shown in Fig. 4b.
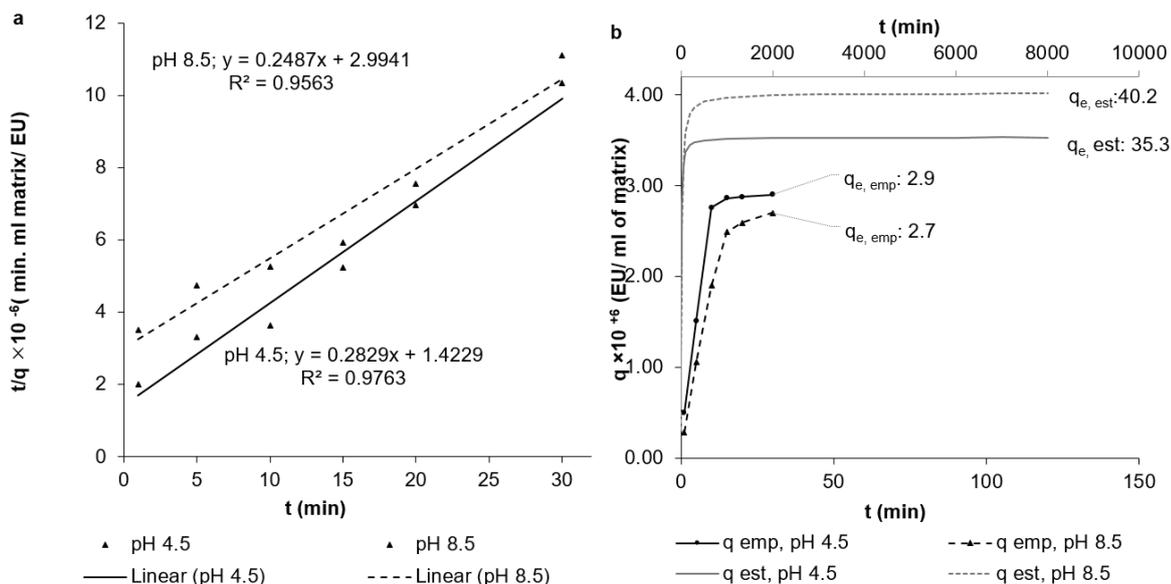

Fig. 4. Kinetic models for studying the reaction order of LPS adsorption. a) Linearized PSO reaction kinetics model: The slope of the trend line was equal to 1/ $q_{e, est}$. Thus, the values of $q_{e, est}$ were calculated 1/0.2487 (4020908.7 EU/ml of the matrix) and 1/0.2829 (3534818.0 EU/ml of the matrix) for pH 8.5 and 4.5, respectively. b) Comparison of LPS adsorption PSO reaction kinetics model with empirical data. At both pHs, the $q_{e, est}$ values were overestimated.

Mass Transfer Models of LPS Adsorption

To determine the rate-controlling mass transfer steps, contributions of intraparticle and pore diffusion steps on the rate of LPS adsorption were evaluated. In well-mixing adsorption systems, especially with high adsorbate concentrations, bulk diffusion occurs fast and is not a rate-controlling step [27]. For modeling the intraparticle diffusion step, according to Equation 8, the q values were plotted versus the square root of time (Fig. 5a) and the equation of the obtained trend line was applied to estimate q_{est}. The comparison of q_{est} with the empirical data is shown in Fig. 5b.
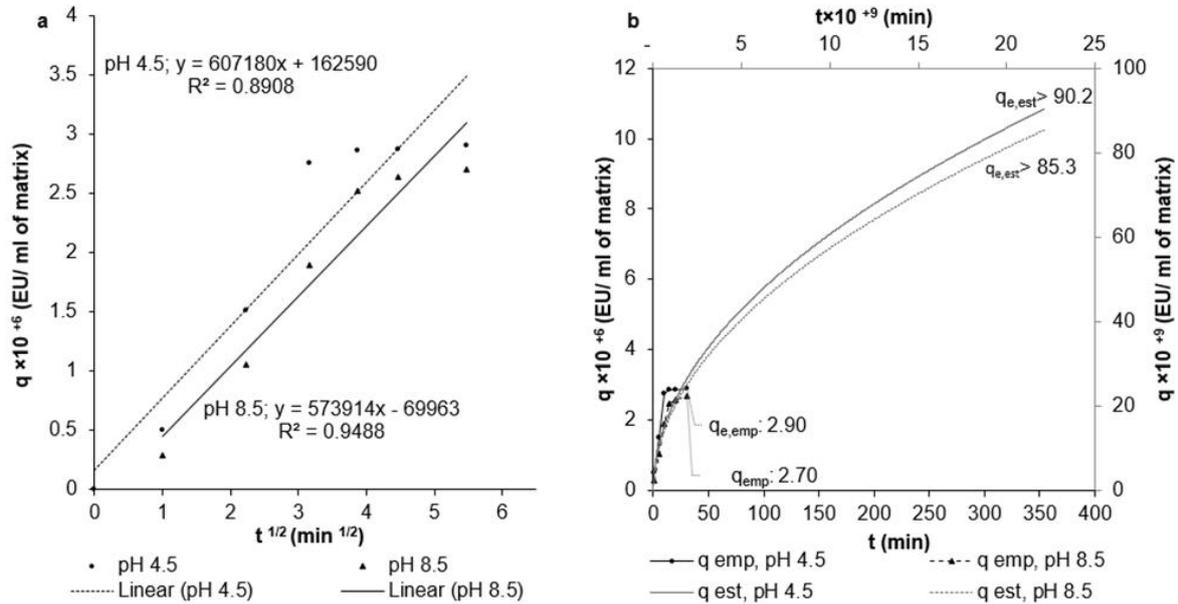
Fig. 5. Intraparticle diffusion mass transfer models of LPS adsorption. a) Weber and Morris' model: The trend lines of both pHs had enough high coefficients of determination (R^2). b) Comparison of LPS adsorption intraparticle diffusion mass transfer model with empirical data. At both pHs, the equilibrium state was not observed and the $q_{t30, est}$ values were overestimated.

As is seen in Fig. 5a, the empirical data of each sample could align through two lines with different slopes. Although fitting empirical data in one line resulted in a high R^2, the resulting models could not estimate the equilibrium state. The intercept of the trend lines for both pHs was not zero. According to Weber and Morris' equation (Equation 8), the intercept is referred to thickness boundary layer constant. Thus, the trend lines not passing the origin (non-zero intercept) indicate the film diffusion could be a rate-controlling step.

For evaluating the applicability of the pore diffusion model, according to the Bangham model (Equation 9), after plotting log (C_0/C_t) values versus log (t), a proper fitting was observed (Fig. 6a). The slope and intercept of the resulting trend lines were used to estimate the LPS concentration in the supernatant at the time of t ($C_{t, est}$). Finally, $C_{t, est}$ was used to calculate q_{est} value according to Equation 1. The comparison of q_{est} with the empirical data and appropriate estimation of equilibrium state are shown in Fig. 6b.
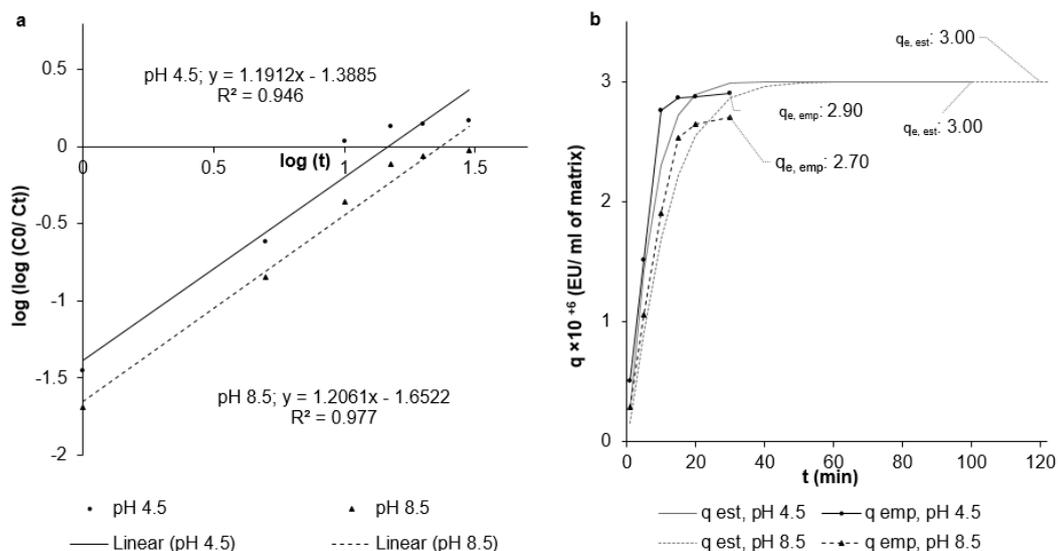
Fig. 6. Pore diffusion mass transfer models of LPS adsorption. a) Bangham model: The trend lines of both pHs had high coefficients of determination ($R^2 > 0.9$). b) Comparison of LPS adsorption pore diffusion mass transfer model with empirical data. For pH 4.5, the equilibrium state was approximately reached, but for pH 8.5, a slight overestimation of q_{t30} value was observed.

Model Fitting Evaluation

The goodness fitting of the discussed models with the empiric model was investigated based on various fitting terms. The coefficient of determination (R^2) obtained from linear regression of models, normalized root mean square error (NRMSE), and relative percentage error (RPE) for qe of all models are listed in Table 1. The coefficient of determination and NRMSE provide measures of closeness of all estimated data to the empirical data and RPE of q_e determines the closeness of $q_{e, est}$ to the $q_{e, emp}$.

Table 1. Error functions applied for investigating the fitting goodness of kinetic models.

Sample	Fitness term	kinetic models				
		Elovich	Pseudo-1st order	pseudo- 2nd order	Intraparticle diffusion	Pore diffusion
S1 (pH 4.5)	R2	0.923	0.951	0.976	0.891	0.946
	NMRSE	0.140	0.229	0.123	0.223	0.122
	RPE (%)	224.02	10.22	21.74	3,109,723.46	3.33
S2 (pH 8.5)	R2	0.950	0.967	0.956	0.949	0.977
	NMRSE	0.134	0.857	0.107	0.170	0.126
	RPE (%)	233.35	48.57	48.79	3,158,002.20	11.02

As shown in Table 1, although the Elovich model overestimated the $q_{e,est}$ too much in both pHs (RPE > 200%), small NRMSE and high coefficients of determination proved good agreement between q_{emp} and q_{est} within the range of incubation times. When comparing the reaction order models, both PFO and PSO reaction models had high R2 and small NRMSE. Although the PFO reaction model could estimate the $q_{e, est}$ of the pH 4.5 sample better than the PSO reaction model (smaller RPE), only the residuals of PSO models of both pHs followed a normal distribution (Table 2). However, the residuals of PFO models for both pHs didn't follow normal distributions (*p*-values < 0.05), indicating that PFO could be a misspecified model or that some influential points affect the model. In contrast, the *p*-values of the normality test for PSO residuals of pH 4.5 and pH 8.5 were 0.826 and 0.843, respectively, representing normal distributions of residuals and proper fitting of PSO models.

Table 2. Normality test of residuals for PFO and PSO models.

Residual	Sample	Shapiro-Wilk		
		Statistic	df	Sig.
PFO models	pH 4.5	0.643	6	0.001
	pH 8.5	0.758	6	0.024
PSO models	pH 4.5	0.961	6	0.826
	pH 8.5	0.963	6	0.843

For evaluating the mass transfer model, the intraparticle diffusion model had smaller R2 and larger NRMSE, representing poor agreement between the estimated values and the empirical data in comparison to the pore diffusion model. Besides, the intraparticle diffusion model did not predict the equilibration state for both S1 and S2 samples and resulted in $q_{e, est}$ values higher than $q_{e, emp}$ values with 3 million relative percentage errors. On the contrary, the small RPE of the pore diffusion model confirmed the suitability of the pore diffusion mass transfer model.

DISCUSSION

This research investigated the kinetics of LPS adsorption on the S3E3-S-Sepharose matrix, an affinity matrix that was generated based on immobilization of S3E3 peptide via thioether bonds on Sepharose 6% chromatography resin. For this purpose, a well-mixed batch-wise process was designed and the amount of adsorbed LPS to the affinity matrix was determined at different contact times. The time-dependent amount of absorbed LPS depicted different adsorption rates showing a sign of multi-rate-controlling mechanisms [10]. Although many articles have investigated the adsorption kinetics of metal ionsm dyes and various chemicals on biomaterial adsorbant [27], there are few cases of studying the adsorption kinetics of biomaterials on any adsorbant . Duarte et,al. studied the adsorption kinetics of BSA on g lignocellulosic adsorbant modifed from eucalyptus bark and vegetable tannins and reported multi-rate-controlling mechanisms including PFO, and intra particle diffusion model [20]. For LPS adsorption kinetics, Lopez and cowrkers reported good fitness of first order reaction model with empirical data of LPS adsorption on metal ion affinity chromatography based on R^2 [28]. In the present study, the models with better R^2, smaller NMRSE, and smaller RPE were selected. Good agreements between the empirical and Elovich model predictive data within the studied incubation range were observed. The Elovich equation is a useful model for heterogeneous adsorbents although it doesn't provide any information about the mechanism of involved chemical reactions. The good fitness of the Elovich equation revealed that the adsorption process was a chemisorption reaction rather than a physisorption [23]. Although the Elovich model could not estimate the q_e properly, the good fitness of the PSO kinetic model proved the chemisorption characteristic of LPS adsorption. The mechanism of LPS interaction with cationic amphiphilic peptides (CAPs) fortifies this finding.

The amphiphilic structure of LPS promotes its binding to the immobilized amphiphilic cationic ligands through ion and hydrophobic interactions [29, 6, 5]. Lipid A is the hydrophobic part of LPS and consists of biphosphorylated β- (1-6)-linked glucosamine disaccharide and 6 fatty acid chains [30]. At pH more than 2.10, (the minimum pKa of phosphate ion) LPS devotes negative charges and binds to the cationic parts of amphiphilic ligands of affinity matrices. Additionally, the hydrophobic fatty acid (acyl) chains of LPS interact with the hydrophobic parts of CAPs [31, 32]. Besides, this chemisorption mechanism of LPS adsorption and the differences between the isoelectric point of immobilized S3E3 peptide (pI 9.43) and the isoelectric point of LPS (pI 2) can explain the relatively higher

amount of adsorbed LPS at lower pH, which was parallel with our previous findings. The immobilized S3E3 peptide had more positive charges at pH 4.5 and could adsorb more LPS in comparison to pH 8.5 [5, 9]. However, the pH of the samples did not affect the type of kinetics model in LPS adsorption.

In this study, both PFO and PSO reaction models could fit empirical data as they had high R2 and small NMRSE. However, by further evaluation based on normality test of residuals, ony PSO model represented normal distributions of residuals which was assign of proper fitting of PSO models. On the contrary, during LPS adsorption on ion metal affinity matrix, a first-order reaction model was reported [28]. This contrast could be because the authors did not evaluate any other model except first order and evaluated the good fitness of model just based on R^2 values.

In this article, the mass transfer mechanism was also studied. The shape of aligned data in the q- t ^{½} plot was a guide for recognizing the mass transfer mechanism. The adsorption process will be controlled by intraparticle diffusion only if the data illustrate a straight line. Otherwise, if the data are aligned through a multi-linear plot, intraparticle diffusion is not the only rate-controlling step (10, 25). In our study, the multilinear plot observed in Fig. 5 indicated that intraparticle diffusion was not the sole rate-controlling mechanism. In addition, the intraparticle diffusion model had a smaller R2 and larger NRMSE, indicating poor agreement between estimated values and empirical data compared to the pore diffusion model. Interestingly, the intraparticle diffusion model failed to predict the equilibration state for both S1 and S2 samples. The estimated $q_{e, est}$ values were significantly higher than the empirical $q_{e, emp}$ values, resulting in large relative percentage errors. In contrast, the small RPE of the pore diffusion model confirmed its suitability as a mass transfer model. Although pore diffusion is one aspect of intraparticle diffusion, it is significant when the pores are the primary pathways for the movement of adsorbates [33].

In conclusion, the kinetics model of LPS adsorption on the S3E3-S-Sepharose affinity matrix was investigated in this study. The experimental data and fitted models revealed that LPS adsorption was a chemisorption reaction and follows from a pseudo-second-order model. Moreover, pore diffusion mass transfer limited the rate of the process. These kinetic findings provide useful information for designing appropriate LPS removal systems during the purification of recombinant biopharmaceuticals and vaccines.

ACKNOWLEDGEMENT

CONFLICT OF INTEREST

The authors declare they have no conflict of interests.

REFERENCES

1. Valentini S, Santoro G, Baffetta F, Franceschi S, Paludi M, Brandini E et al. Monocyte-activation test to reliably measure the pyrogenic content of a vaccine: An in vitro pyrogen test to overcome in vivo limitations. Vaccine. 2019;37(29):3754-60. doi:https://doi.org/10.1016/j.vaccine.2018.10.082.
2. Sanders H, Kaaijk P, Van Den Dobbelsteen GP. Preclinical evaluation of MenB vaccines: prerequisites for clinical development. Expert review of vaccines. 2013;12(1):31-42.
3. Williams KL. Endotoxins: pyrogens, LAL testing and depyrogenation. CRC Press; 2007.

4. Hirayama C, Sakata M. Chromatographic removal of endotoxin from protein solutions by polymer particles. J Chromatogr B Analyt Technol Biomed Life Sci. 2002;781(1-2):419-32. doi:https://doi.org/10.1016/s1570-0232(02)00430-0.
5. Sepahi M, Hadadian S, Ahangari Cohan R, Norouzian D. Lipopolysaccharide removal affinity matrices based on novel cationic amphiphilic peptides. Preparative Biochemistry & Biotechnology. 2020:1-9. doi: https://doi/org/10.1080/10826068.2020.1821216.
6. Li J, Shang G, You M, Peng S, Wang Z, Wu H et al. Endotoxin removing method based on lipopolysaccharide binding protein and polyhydroxyalkanoate binding protein PhaP. Biomacromolecules. 2011;12(3):602-8. doi:https://doi.org/10.1021/bm101230n.
7. Todokoro M, Sakata M, Matama S, Kunitake M, Ohkuma K, Hirayama C. Pore-size controlled and poly(e-lysine)-immobilized cellulose spherical particles for removal of lipopolysaccharides. Journal of Liquid Chromatography & Related Technologies. 2002;25(4):601-14. doi: https://doi.org/10.1081/jlc-120003349.
8. Sepahi M, Ahangari Cohan R, Hadadian S, Norouzian D. Effect of glutamic acid elimination/substitution on the biological activities of S3 cationic amphiphilic peptides. Preparative Biochemistry and Biotechnology. 2020;50(7):664-72. doi: https://doi.org/10.1080/10826068.2020.1725772.
9. Sepahi M, Norouzian D, Cohan RA, Hadadian S. Optimization of the Endotoxin Removal Performance of Solid-Phase Conjugated S3E3 Antimicrobial Peptide Using Response Surface Methodology. International Journal of Peptide Research and Therapeutics. 2021:1-9. doi: https://doi/org/10.1007/s10989-021-10230-y.
10. Bilgili MS. Adsorption of 4-chlorophenol from aqueous solutions by xad-4 resin: isotherm, kinetic, and thermodynamic analysis. Journal of Hazardous Materials. 2006;137(1):157-64.
11. Yu Q, Zhang R, Deng S, Huang J, Yu G. Sorption of perfluorooctane sulfonate and perfluorooctanoate on activated carbons and resin: kinetic and isotherm study. Water research. 2009;43(4):1150-8.
12. Schaumberger S, Ladinig A, Reisinger N, Ritzmann M, Schatzmayr G. Evaluation of the endotoxin binding efficiency of clay minerals using the Limulus Amebocyte lysate test: an in vitro study. AMB Express. 2014;4(1):1.
13. Li J, Zhang Y, Ping Z, Li M, Zhang Q. Synthesis and endotoxin removal properties of a novel affinity sorbent with poly (1-vinylimidazole) as the ligand. Process Biochemistry. 2011;46(7):1462-8.
14. Sawada Y, Fujii R, Igami I, Kawai A, Kamiki T, Niwaf M. Endotoxin removal from water using microporous polyethylene chopped fibres as a new adsorbent. Epidemiology & Infection. 1986;97(1):103-14.
15. Razdan S, Wang J-C, Barua S. PolyBall: A new adsorbent for the efficient removal of endotoxin from biopharmaceuticals. Scientific Reports. 2019;9(1):8867. doi: https://doi.org/10.1038/s41598-019-45402-w.
16. Zhang Y, Yang H, Zhou K, Ping Z. Synthesis of an affinity adsorbent based on silica gel and its application in endotoxin removal. Reactive and Functional Polymers. 2007;67(8):728-36.
17. Lonza08291. Limulus Amebocyte Lysate (LAL) QCL-1000™. 2014.
18. Najafi M, Yousefi Y, Rafati A. Synthesis, characterization and adsorption studies of several heavy metal ions on amino-functionalized silica nano hollow sphere and silica gel. Separation and Purification Technology. 2012;85:193-205. doi:https://doi.org/10.1016/j.seppur.2011.10.011.
19. Bensalah J, Doumane G, Iraqi O, Elhenawy AA, Ouaddari H, Okla MK et al. Optimization of an experimental study of cationic Pb metal adsorption by resin polymer. Scientific Reports. 2023;13(1):20060. doi: https://doi.org/10.1038/s41598-023-46967-3.
20. Duarte DS, Luzardo FH, Velasco FG, de Almeida ON, Bedon GD, Nascimento GG et al. Adsorption of BSA Protein in Aqueous Medium Using Vegetable Tannin Resin from Acacia mearnsii (Mimosa) and Modified Lignocellulosic Fibers from the Bark of Eucalyptus citriodora. Journal of Polymers and the Environment. 2023;31(8):3418-32.
21. He Y, Wu P, Xiao W, Li G, Yi J, He Y et al. Efficient removal of Pb(II) from aqueous solution by a novel ion imprinted magnetic biosorbent: Adsorption kinetics and mechanisms. PLOS ONE. 2019;14(3):e0213377. doi: https://doi.org/10.1371/journal.pone.0213377.
22. Sukeesan S, Boontanon N, Fujii S, Boontanon SK. Evaluation of the adsorption behavior of mixed perfluoroalkyl and polyfluoroalkyl substances onto granular activated carbon and styrene-divinylbenzene resins. Remediation Journal. 2023;33(4):297-308. doi: https://doi.org/10.1002/rem.21766.

23. Yuan X, Choi SW, Jang E, Lee KB. Chemically activated microporous carbons derived from petroleum coke: Performance evaluation for CF4 adsorption. Chemical Engineering Journal. 2018;336:297-305.

24. Lima ÉC, Adebayo MA, Machado FM. Kinetic and equilibrium models of adsorption. Carbon nanomaterials as adsorbents for environmental and biological applications. 2015:33-69.

25. Kang H-J, Kim J-H. Adsorption kinetics, mechanism, isotherm, and thermodynamic analysis of paclitaxel from extracts of Taxus chinensis cell cultures onto Sylopute. Biotechnology and Bioprocess Engineering. 2019;24(3):513-21.

26. Richter K, Hank TB, Atzberger C, Mauser W, editors. Goodness-of-fit measures: what do they tell about vegetation variable retrieval performance from Earth observation data. Remote sensing for agriculture, ecosystems, and hydrology XIII; 2011: International Society for Optics and Photonics.

27. Mohamed Nasser S, Abbas M, Trari M. Understanding the rate-limiting step adsorption kinetics onto biomaterials for mechanism adsorption control. Progress in Reaction Kinetics and Mechanism. 2024;49:14686783241226858. doi: https://doi.org/10.1177/14686783241226858.

28. Lopes AM, Romeu JS, Meireles RP, Perera GM, Morales RP, Jr AP et al. Adsorption of endotoxins on Ca2+ iminodiacetic acid by metal ion affinity chromatography. Chinese journal of chromatography. 2012;30(11):1194.

29. Ding JL, Zhu Y, Ho B. High-performance affinity capture-removal of bacterial pyrogen from solutions. Journal of Chromatography B: Biomedical Sciences and Applications. 2001;759(2):237-46. doi: https://doi.org/10.1016/S0378-4347(01)00227-4.

30. Ongkudon CM, Chew JH, Liu B, Danquah MK. Chromatographic removal of endotoxins: a bioprocess engineer's perspective. ISRN Chromatography. 2012;2012.

31. Li P, Wohland T, Ho B, Ding JL. Perturbation of lipopolysaccharide (lps) micelles by sushi 3 (s3) antimicrobial peptide the importance of an intermolecular disulfide bond in s3 dimer for binding, disruption, and neutralization of lps. Journal of Biological Chemistry. 2004;279(48):50150-6. doi: https://doi.org/10.1074/jbc.M405606200.

32. Teixeira V, Feio MJ, Bastos M. Role of lipids in the interaction of antimicrobial peptides with membranes. Progress in lipid research. 2012;51(2):149-77. doi:https://doi.org/10.1016/j.plipres.2011.12.005.

33. Silva LM, Munoz-Pena MJ, Domínguez-Vargas JR, González T, Cuerda-Correa EM. Kinetic and equilibrium adsorption parameters estimation based on a heterogeneous intraparticle diffusion model. Surfaces and Interfaces. 2021;22:100791. doi: https://doi.org/10.1016/j.surfin.2020.100791.